DRAFT

LABORATORY MEASUREMENTS OF THE EVOLUTION OF A VORTEX PAIR IN A NONSTRATIFIED FLUID

By

Donald P. Delisi[1],
George C. Greene[2],
Donald B. Altman[1],
Lee E. Piper[1], and
Raminder Singh[3]

[1]Northwest Research Associates, Inc.
P.O. Box 3027
Bellevue, WA 98009

[2]NASA Langley Research Center
Hampton, VA

[3]Indian Institute of Technology
Kanpur, India

April 1992

DRAFT

ABSTRACT

New measurements of the evolution of a vortex pair from a lifting wing in a nonstratified fluid are presented. The new feature of these measurements is the use of nearly neutrally buoyant particles as the primary flow visualization tool. Using dye, as in previous studies, we show that our results are consistent with observations of other researchers. Using particles, however, organized vorticity is shown to persist for significantly longer times and to migrate significantly longer distances than observed in previous studies. The vortex motion is observed in three stages: (1) a two-dimensional line vortex pair, (2) transition from two-dimensional to three-dimensional vorticity via a mutual induction, or Crow, instability, and (3) vortex rings. Unlike previous studies, the third stage of vortex rings is shown to be very stable and robust. In nondimensional units of time, T, the first stage is shown to last until $T \approx 5$, the second stage from $T \approx 5$ to ≈ 11, and the third stage from $T \approx 11$ to at least 100. Characteristics of the flow are measured for each stage in the evolution. Practical implications for commercial aircraft wakes are also discussed.

1. Introduction

Vorticity from the wings of an aircraft in flight rapidly rolls up into a trailing wake vortex pair. Understanding the evolution of this vortex pair has important applications in aircraft operations, such as maximizing the capacity of crowded airports.

Vortex evolution has been studied experimentally, numerically, and theoretically for many years. For some of the many reviews available, see Hall (1972), Widnall (1975), Leibovich (1978), Saffman and Baker (1979), Smith (1986), and Sarpkaya (1989). In spite of this extensive research, our knowledge is still rather limited. Much of our current knowledge of high Reynolds number vortex evolution is from measurements of aircraft flight data where detailed measurements are difficult to make (see, e.g., Olsen et al, 1971; Tombach, 1973; Burnham et al, 1978; and Burnham, 1982). These studies suggest maximum limits on both the vertical migration distance of the vortices and on their lifetimes. For example, it was found that Boeing-747 vortex wakes migrated a maximum vertical distance of about 900 ft (Condit and Tracy, 1971). Typically, however, meteorological measurements to quantify ambient background effects, such as stratification, turbulence, and shear, were not made during these vortex observations. Also, smoke was used as the primary flow visualization tool (alternately, the observations were taken using more sophisticated, ground-based sensors, but the vortices were in or near ground effect).

To measure the effect of the ambient environment under controlled conditions, several investigators performed vortex evolution studies in the laboratory (Barker and Crow, 1977; Tomassian, 1979; Sarpkaya, 1983; Sarpkaya and Daly, 1987). These studies all used observations of dye in the vortex cores as the primary measurement of vortex migration, and they also found maximum limits on vortex migration distance and lifetime. Taken together, they found that the maximum vertical migration occurred for nonstratified, quiescent flows, and that

ambient stratification and/or ambient turbulence decreased the observed maximum migration distance and lifetime.

For measurements of vortex wake motion, the full-scale flight tests and the laboratory observations are in rough agreement. If we use a nondimensional vertical migration distance, $H = h / b_0$, where h is the vertical distance the vortex has migrated in time t ($h = 0$ at $t = 0$) and b_0 is the initial vortex separation, the above full-scale observations suggested that the maximum value of H, H_{max}, is about 6, and the laboratory studies observed H_{max} of about 6.5. If we define a nondimensional vortex time, $T = V_0 t / b_0$, where V_0 is the initial vortex migration velocity, the above laboratory studies indicated that T_{max} was about 9. Note that both the full-scale measurements and the laboratory observations used dye or smoke as the flow visualization method.

Recently, Delisi and Greene (1990) reported on laboratory studies of vortex evolution in nonstratified flows using both dye and neutrally buoyant particles as the flow visualization methods. They found that dye and particles gave identical results for early vortex evolution times, but that particle observations suggested that organized vorticity migrates much farther and lasts much longer than was observed using dye. In their study, Delisi and Greene (1990) were unable to determine the maximum vertical migration distance and lifetime of the vortices due to the finite depth of their laboratory facility.

The purpose of this paper is to expand on the study of Delisi and Greene (1990). Here, we will show that previous laboratory studies using dye in a nonstratified, quiescent flow underpredicted the maximum vertical migration distance of organized vorticity by a factor of at least four, and underpredicted vortex lifetime by a factor of at least ten. We will also characterize some of these late vortex flows.

In Section 2, we discuss the experimental facility. Results are presented in Section 3, and a discussion is given in Section 4. Concluding remarks are given in Section 5.

2. The Experimental Facility

2.1 Description of the Apparatus

The experiments were performed in a towing tank measuring 9.8 m long, 0.9 m wide, and 1.0 m deep. The tank was filled with nonstratified fresh water to a depth of 0.9 m.

Vortices were generated by horizontally towing lifting wings down the tank. The wings were towed near the water surface, and the resulting vortices propagated vertically downwards toward the floor of the tank. The wings were supported by thin struts which extended through the water surface. Typically, the chord of the strut was 13 mm and the thickness of the strut was 1.6 mm. The strut was attached to a carriage at the top of the tank which travelled down the tank at constant speeds up to 324 cm/sec. It was found that, at high carriage speeds with the wing close to the surface, air travelled down the strut and into the trailing vortices. To eliminate this ventilation, the trailing edge of the strut was beveled.

A family of wings of rectangular planform and aspect ratio of approximately two were used in this study. Because we wanted to investigate how far vortices propagated, we wanted to use as small a wing span as possible, in order to have as large a nondimensional depth, 4, as possible. However, we also wanted the strut holding the wing to have a minimal effect on the flow field around the wing. Thus, the smallest wing we tested had a span of 3.8 cm. Table 1 lists the physical parameters of the wings and the maximum chord Reynolds numbers, Re_c, where $Re_c = Uc / \nu$, U is the average towing speed, c is the chord of the wing, and ν is kinematic viscosity.

2.2 Flow Visualization and Measurements

Flow visualization was performed with fluorescein dye and nearly neutrally buoyant particles. The dye was used to visualize the initial vortex cores for measurements of b_o. For

these measurements, fluorescein powder was mixed with Liquitex (Sarpkaya, 1983), and the resulting paste was applied in several thin coats to transparent tape. The tape was then cut to shape and placed on the wing tips, resulting in a dyed vortex core when the wing was towed in the tank. The dyed cores were photographed with 35-mm cameras and/or video taped with a camcorder.

Particles were also used to visualize the flow field (Delisi and Dunkerton, 1989; Delisi and Greene, 1990). The density of the particles was slightly greater than fresh water, resulting in an average sinking of the particles at a rate of approximately 1 - 2 mm/sec. The particles were used in three ways. First, the particles were seeded uniformly in the tank, and visualized with a light slit oriented perpendicular to the path of the wing. A 35-mm camera then took time exposures of the resulting flow, resulting in streak photographs. An example is given in Figure 1. In this photograph, the view is from a camera located inside the tank looking upstream. The wing direction is out of the page and the vertical light sheet is perpendicular to the path of the wing. Since the wing is generating positive lift, the resulting vortex system is propagating downwards, towards the floor of the tank. Thus, the particles in the left (right) vortex in Figure 1 are rotating in a clockwise (counterclockwise) direction. Note that, with this flow visualization technique, the vortices are well visualized. Estimates of the vortex migration distance and core-to-core separation were read manually from these streak photographs. Second, particles were introduced into a clear tank only at the surface. When the particles sank to the depth of the wing, the wing was towed down the tank and particles were entrained into the vortices. For these experiments, a vertical light sheet was oriented parallel to the path of the wing and a 35-mm camera and camcorder looking at the side of the tank recorded the streak photographs and video images, respectively. An example of these streak photographs is given in Section 3.3. Finally, particles were distributed uniformly on the bottom of the tank by allowing time for the particles in the water to settle to the bottom. With this technique, the wing is towed down the tank, vortices propagate downwards towards the tank floor and scour the floor, moving the particles.

Photographs of the tank floor thus record the integrated effect of the vortex motion on the particles. Photographs of the tank floor using this technique are also shown in Section 3.3.

Wing lift and towing speed were measured during each run. Lift was measured using a piezoelectric force transducer attached to the wing strut mount. The output of the transducer was digi ed and stored on a personal computer. The lift transducer was calibrated prior to the series of experiments, and the calibration was checked periodically by measuring the lift of a standard wing at a standard speed and angle. For nominally identical runs, lift measurements were repeatable to within 3 percent.

Towing speed was determined by measuring the time needed for a 10-cm long rod, connected to the carriage, to pass through a photodetector. The average towing speed was based on measurements at three positions in the test section during each run. For nominally identical runs, at all speeds, the average speed through the test section was constant and repeatable to within ± 1 cm/sec.

3. Results

3.1 Lift Measurements

For each wing, we obtained a coefficient of lift, angle of attack (C_L- α) curve, where

$$C_L = \frac{L}{1/2\ \rho U^2 A},$$

L is lift, ρ is density, A is the wing area, and α is the angle of attack. The purpose of obtaining a C_L - α curve was to confirm that we were not taking measurements near aerodynamic stall. For these wings, aerodynamic stall occurred around 22 deg; a typical angle of attack used in this study was 13 deg.

In order to provide the maximum possible vertical propagation distance for the wake vortices, the wings were towed as close as technically feasible to the free surface. To determine the effect of the free surface on the generation of lift, we measured lift with wings at different depths below the water surface, keeping towing speed and angle of attack constant. Figure 2 shows the measured lift, normalized by the lift at a depth of 2 spans, vs trailing edge depth, in wing spans, for two wings and two towing speeds. The un-normalized lifts vary by a factor of over three for the data in Figure 2. The normalized lifts shown in Figure 2, however, collapse to a single curve which shows a similar trend for each wing and towing speed. Figure 2 shows that the minimum depth for which full lift is generated is around 1.5 wing spans. For the results presented here, all data were taken with the trailing edge at a depth of at least 1.5 spans.

3.2 Measurements of b_0 and V_0

Measurements of b_0 were obtained using dye on the airfoil to visualize the vortex cores. For an eliptically-loaded wing, b_0 is $\pi/4$, or 78 percent, of the wing span. For the wings used in this study, b_0 was measured to be between 83 and 86 percent of the wing span.

V_0 is the vertical velocity of the centroid of the vorticity shed from the wing. This is not necessarily the same as the vertical velocity of the tip vortex cores prior to complete wake rollup.

Estimates of V_0 were obtained in two steps. First, measurements of the depth of the vortex cores vs time were obtained both from in-tank photographs of particle streaks and from side views of particles. Second, a linear least squares fit through this height vs time data for $H < 3.5$ yielded V_0.

An accurate determination of V_0 is more difficult than it first appears, since the value of V_0 is sensitive to the manner in which the least squares fit is performed. We found that if we constrained the fit to pass through the trailing edge depth at $t = 0$, the residuals of the least squares fit were large, and the fit was not accurate. If we ignored the constraint, the fit was

accurate, but, for each run, we had an "effective origin" of the vortex. We eventually chose to not constrain the least squares fit to pass through the trailing edge of the wing at time t = 0, resulting in an effective origin either above or below the wing trailing edge. For the runs used in this study, the median absolute vertical position of this "effective origin" was 1.1 cm from the trailing edge of the wing.

For nominally identical runs, V_0 calculated using the above procedure was repeatable to within 5 percent.

3.3 Measurements of Vortex Migration and Lifetime

Figure 3 is adapted from Delisi and Greene (1990) and shows dye observations of nonstratified vortex motions. In this figure, the "plus" symbols show data from Tomassian (1979), who generated two-dimensional vortices, and the "Xs" are from Sarpkaya (1983), who generated three-dimensional vortices using wings in a towing tank. The circles are our dye observations of three-dimensional vortices. This figure shows that our dye observations are essentially consistent with those of previous investigators.

Delisi and Greene (1990) showed that when nearly neutrally buoyant particles are used for flow visualization, the observations can continue beyond those shown in Figure 3. Figure 4 shows a series of streak photographs of these particles for one run. In this figure, the flow is being viewed from the side of the tank, and the flow is illuminated with a vertical light sheet along the wake centerline. The wing has moved from left to right at the top of the tank, and the particles were added only in the very top layer of the tank near the water surface. As the vortices propagate vertically downwards into the tank, some of the particles are entrained by the vortices. In the first photograph in this figure, Figure 4a, the trailing wake is a two-dimensional line vortex pair, from left to right, at the bottom edge of the region with particles. In Figure 4b, the wake is beginning to show some nonuniformity axially. Note the downward propagation of the

wake with each succeeding photograph. In Figure 4c, the wake is becoming distinctly three-dimensional. In Figure 4d, three vortex rings have evolved from the two-dimensional line vortex pair. The rings are being cut down the center by the light sheet, with half the ring on each side of the sheet. (The light sheet is, in essence, cutting a doughnut-shaped vortex in half.) Thus, each of the three vortex pairs shown in Figure 4d is the center slice of a ring vortex. The remaining photographs, Figures 4e - 4h, show the vertical migration of these three-dimensional rings, essentially unchanged, to the bottom of the tank.

Note in Figure 4h that the particles, which were initially only near the water surface, are now nearly uniformly distributed in the upper half of the tank. In the lower half of the tank, the particles appear in columns, where they have been transported by and diffused out of the rings. Note that, by comparing Figure 4h to Figure 4e, the average sink rate of the particles is small compared to the time scale of the flow field. (Compare, for example, the depths of the tops of the regions containing no particles.) Thus, we believe that, although the particles are slightly heavier than the fresh water, their slow sinking is not significantly affecting the evolution of the flow.

Figure 5 shows drawings of the flow fields in Figure 4 at two times in the evolution. For each of the two times, there is a three-dimensional view and a side view. The side view shows schematically what would be observed using a light sheet on the centerline of the wake, similar to the photographs in Figure 4.

Figures 5a and 5b show the three-dimensional and side view, respectively, for the early evolution corresponding to Figure 4a. Here, the flow is two-dimensional, and the line vortex pair, when viewed from the side, results in vertical motion only at the bottom of the region containing particles. (For clarity, the particles transported but left by the vortices have not been drawn in Figure 5, although they are seen in the photographs in Figure 4.) Figures 5c and 5d show the same views at a later time in the evolution. By this time, three-dimensional rings have

formed from the two-dimensional line vortex pair. The side view, Figure 5d, shows just the slice down the centerline and shows one vortex pair associated with each ring. These vortex pairs are no longer two dimensional but are, instead, the visualization resulting from a two-dimensional light sheet passing through three-dimensional rings. Note that the diameter of the ring, D, is much smaller than the distance between rings, d. The flow shown in Figures 5c and 5d corresponds to the flow in Figures 4d to 4h.

The 2-D to 3-D evolution visualized in Figures 4 and 5 is the well-known mutual induction, or Crow, instability which was identified by Scorer (1958) and analyzed by Crow (1970). Tombach (1973) observed that Crow instability occurs infrequently (at least for the small, propeller-driven aircraft used in his study) and that vortex bursting more often destroys the vortices before Crow instability occurs. These aircraft observations were obtained, however, using smoke to track the aircraft wake vortices. In our laboratory experiments, dye in the vortex cores indicates that vortex bursting *often occurs before* Crow instability. However, our observations of particle motions show that vortex bursting does not prevent Crow instability. Rather, Crow instability always occurs, either before or after bursting, and the resulting ring vortices propagate to the floor of the tank.

A different view of the vortex evolution is shown in Figure 6. Here, we show photographs of the bottom floor of the tank after the vortex motion has disturbed an initially uniform distribution of particles on the tank floor. In Figure 6a, the wing was at a height of 2.5 spans above the floor, and the edges of the disturbance on the floor are nearly straight, indicating that the disturbance is nearly two-dimensional. In Figure 6b, the wing was at a height of 5 spans above the floor. Now, the edges of the disturbance on the floor are wavy, indicating the onset of Crow instability. In Figure 6c, the wing was at a height of 8 spans, and the disturbances are distinctly three-dimensional. These photographs corroborate the observations in Figure 4, although they were made with a different wing and a different towing speed.

In Figure 7, we plot H vs T for the run shown in Figure 4. The letters at the bottom of this figure correspond to the appropriate photographs in Figure 4. Note that the wake is two-dimensional up to around T ≈ 5, the instability occurs around T ≈ 5 to 10, and three-dimensional vortices persist for T > 10.

Since each of the vortex rings shown in Figure 4 are about the same diameter and propagate vertically at nearly the same rate, they are of nearly equal strengths. This is not, however, what we normally observed. Typically, the two-dimensional wake vortices will exhibit little scatter on an H vs T plot, but the vortex rings will exhibit considerable scatter due to differing vertical migration velocities. An example is shown in Figure 8. Here we show, for one run, H vs T for two regions of the test section. The left center (right center) part of the test section is shown as the circles (squares). A three-dimensional ring vortex evolved in each of these two parts of the test section. For early times, the scatter between the two measurements is small. At later times, however, the scatter grows until it is quite large. At the last measurement, at H = 16.8, T_{left} = 34.7 while T_{right} = 53.3, and there is considerable scatter.

A composite of all our H vs T data for the 5.1 cm span wing is shown in Figure 9. Here, the circles are for a chord Reynolds number of 82,300, the squares are for a chord Reynolds number of 58,900, and the triangles are for a chord Reynolds number of 44,700. For these experiments, the bottom floor was at H ≈ . Thus, all these measurements end due to the finite tank depth.

Figure 10 shows data similar to that in Figure 9 for the 3.8 cm span wing. Many of the runs with this wing were performed with the wing at a depth of 5 spans. Thus, many of the measurements in Figure 10 end at H between 15 and 17. (Although the distance between the wing and the bottom floor is H ≈ 22, the particles, when viewed from the side of the tank, can only be observed to around H ≈ 17.) In three of the runs with this wing, however, the wing was at a depth of 1.5 spans (floor at H ≈ 26). For these three runs, the data in Figure 10 go to H ≈ 22

with corresponding values of T from 61 to 116. These experiments, then, are also facility-limited, and do not show the maximum values of eight H or T.

3.4 Vortex Ring Merging

Figure 11 shows the time history of the bottom of the region containing particles in Figure 4. Initially, we see a nearly-horizontal straight line propagating downwards, as the two-dimensional wake vortex migrates vertically. Then, around T ≈ 5, the two-dimensional wake starts to become three-dimensional. Thereafter, the three-dimensional vortex rings form and propagate to the bottom of the tank.

The experiment shown in Figure 11 was unusual in that equally-spaced rings formed and persisted for the duration of the experiment. Figure 12 shows the time history of the bottom of the particle-laden region for a more typical experiment. Here, the two-dimensional vortex wake becomes unstable, as in Figure 11, but there is now some merging of three-dimensional motions. Note, for example, how the two initial perturbations on the left side of Figure 12 merge into one ring. A similar merging occurs on the right side of Figure 12, although at a later time.

The merging of vortex rings is, of course, not a new phenomena and has been studied in detail recently both numerically (Aref and Zawadzki, 1991) and experimentally (Schatzle, 1987). Arefand Zawadzki (1991) simulated vortex ring merging for conditions similar to those reported in Schatzle (1987) and found, as in the experiment, that after merging the vortices separated in a plane perpendicular to the original plane of motion. This separation after merging was not observed in the current experiments. A complete understanding of when separation after merging will occur does not exist but it is known to be sensitive to the initial conditions, particularly the approach angle of the vortices.

The bottom of the particle-laden region, as traced in Figures 11 and 12, shows the instabilities in the wake as they develop. If we plot the distance, d, between the instabilities for

Figure 12, d will decrease between the structures that are merging and increase between the surviving structures. Figure 13 shows these distances for the experiment shown in Figure 12. Here, we see low values of d / b_0 at early time for the merging structures, and higher values later for the resulting structures. Figures 14 and 15 show similar data for all the runs for the 3.8 cm and 5.1 cm span wings, respectively. Note from these figures that the trend is for d to increase with time, reflecting the merging of the vortices. At times later than T = 30, the data show d / b_0 to be more nearly constant. These data, however, are for a small number of runs. Hence, our data set for d / b_0 at late times is limited, and the values shown for d / b_0 for long times should, at this time, be viewed cautiously.

The straight lines in Figures 14 and 15 are least squares fits through the data for $T < 30$. The original theory for mutual induction instability by Crow (1970) showed that the most unstable wavelength was $d / b_0 = 8.6$. From Figures 14 and 15, at T = 5, the least squares fit gives d / b_0 of 5.3 for the 3.8 cm span wing and 5.5 for the 5.1 cm span wing. Both of these values are lower than the value predicted by Crow. From visual observations of particles from the side of the tank (similar to Figure 4), we have determined that the three-dimensional structures are fully formed between T of 10 and 12. Using T = 11 as the average time of fully developed three-dimensional ring vortices, the least squares fits at T = 11 give $d / b_0 = 6.7$ for the 3.8 cm span wing and 7.1 for the 5.1 cm span wing. The values from Figures 14 and 15 at T = 11, along with estimates for the 10.2 cm span wing from photographs of bottom particle displacements (similar to Figure 6), are plotted in Figure 16. Note that these values are all somewhat smaller than the value predicted by Crow (1970).

3.5 Measurements of Vortex Ring Diameter

Diameters of the ring vortices versus time were measured from particle streak photographs such as those shown in Figure 4. The ring diameters, D, normalized by b_0, are presented in Figure 17 for both the 3.8 cm and the 5.1 cm span wings. These data show that

there are no apparent differences in the normalized ring diameters between the two wings, and that the ring diameters remain relatively constant with time. The slow increase in ring diameter shown in Figure 17 is consistent with the results of Glezer and Coles (1990) who measured vortex ring diameters at one station downstream of a vortex-ring generator. Solid symbols in Figure 17 represent rings that have merged and re-formed. These merged rings have nearly the same diameters as the initial, unmerged rings. Apparently, ring diameters are substantially larger than those shown in Figure 17 only during initial formation from the two-dimensional wake and during merging.

4. Discussion

The choice of dye or neutrally buoyant particles for flow visualization results in vastly different interpretations of the evolution of a vortex pair. Using dye, the vortex motion cannot be visualized beyond $H \approx 6$ and $T \approx 9$ (Figure 3). Using particles, however, we can follow organized, 3-D vortex structures to at least $H \approx 22$ and $T \approx 100$ (Figure 10). Note that these larger values are themselves not the maximum vortex migration distances or the maximum vortex lifetimes, since, for the smallest wing, the vortices usually (but not always) hit the bottom of the tank, at $H = 26$.

Our results illustrate the difficulty of correctly interpreting fluid motions from flow visualization results. The perception of local dye movement is a function of both dye concentration (how much dye is present) and dye contrast (how easily the dye is distinguished from the surrounding fluid). If the dye concentration is weak, or if the concentration is uniform, no local motion can be perceived. The concentration of dye at a particular location and time is an integrated effect of mass transport and diffusion between the times when the dye is introduced to the flow and when it is observed. Consequently, tracking dye for long periods of time implies longer integration times. If these time periods are long enough, the dye concentrations are low

and may not be observable. Similarly, the motion of the dye may not be observed if the gradients in dye concentration are small.

Like dye, the number of particles in a given volume at a given time is an integrated effect of mass transport and diffusion. Also like dye, the concentration of particles in the vortices decreases with time. Particles, however, remain intact. Proper lighting allows each particle to have a high contrast with the background, and the resulting flow field can be observed in a streak photograph even at late times. Thus, although the concentration of particles in the vortices is lower in Figure 4h than in Figure 4a, both photographs show the vortical motions. A fundamental difference between dye and particles, then, is that there is a minimum concentration and gradient of dye necessary for observation while almost any concentration of particles (other than no particles or complete saturation) is acceptable for streak photographs. This fundamental difference between dye and particles allows vortex motions to be observed using particles for substantially longer times than observations using dye.

Particles are useful for visualizing the flow in several planes. For early times, the cross-track plane (e.g., Figure 1) enables the simultaneous measurement of both vortex depth and core separation. At later times, the flow is no longer two-dimensional, and the cross-track plane may or may not slice through the three-dimensional rings, depending on the along-track position of the rings. Consequently, at later times the flow is best observed with along-track visualization (e.g., Figure 4). Bottom particle photographs give yet a third view of the evolution (e.g., Figure 6).

The most unanticipated result of our study is the apparent universality of Crow instability and the apparent long-lived nature of the resulting three-dimensional vortex rings. Previous full-scale and laboratory studies have observed Crow instability (e.g., Condit and Tracy, 1971; Sarpkaya, 1983), but the smoke (full-scale) or dye (laboratory) diffused quickly once rings were formed, giving the impression that the vorticity had decayed to negligible levels. The long-lived

nature of the resulting vortex rings is not surprising, based on their stability (Glezer and Coles, 1990). However, the fact that there have been no previously documented examples of 2-D line vortices evolving into long-lived, 3-D ring vortices is evidence of the difficulty in correctly interpreting flow visualization results.

We have documented three distinct flow fields in the evolution of the trailing wake vortex behind a wing: the 2-D line vortex pair, the transition region, and 3-D ring vortices. From side views of particle motions, we have estimated for each run the time we first visually observed an instability in the line vortex pair and the time the three-dimensional vortices are completely formed. These results are shown in Figure 18 which is a pictorial summary of the results from both the 3.8 cm and 5.1 cm wings (circles and squares.) Note that the results are similar for both wings.

5. Comments

The results presented here have important implications on our understanding of vortex motion behind a wing. Below, we briefly summarize our views of the current state of understanding of vortex evolution.

H_{max} and T_{max}

Due to the depth of our experimental tank, we did not measure either H_{max} or T_{max}. From Figure 10, however, for low Reynolds number wake vortices in a nonstratified, nonturbulent, nonsheared flow, H_{max} is at least 22 and T_{max} is at least 100.

Effect of Reynolds Number

In our study, Re_c was less than 189,200. In contrast, for commercial airplanes in level flight, Re_c is typically several tens of millions. According to Greene (1986), high Reynolds number vortices will migrate farther and last longer than low Reynolds number vortices. Thus, we expect both H_{max} and T_{max} to increase with Reynolds number. Quantitatively, the only known estimate for the amount of increase is given by Greene (1986).

Effect of Ambient Stratification and Turbulence

From previous laboratory studies, we expect H_{max} and T_{max} to decrease with increasing stratification and/or increasing turbulence (Tomassian, 1979; Sarpkaya, 1983; Sarpkaya and Daly, 1987). However, these studies all used dye to track the vortex motion, and they all underestimated both H_{max} and T_{max} in a nonstratified, nonturbulent flow. Thus, although we believe H_{max} and T_{max} will decrease with increasing stratification and/or increasing turbulence, we

believe one cannot quantitatively estimate the amount of change in either H_{max} or T_{max} with the change in stratification or turbulence from prior results.

Effect of Ambient Shear

Robins and Delisi (1990) recently reported on numerical studies of vortex evolution in flows with both stratification and shear and found that, under some conditions, vortices decayed slower and lasted longer with shear than in the absence of shear. Furthermore, Delisi et al (1991) reported on laboratory measurements of vortex evolution in a stratified shear flow and supported the findings of Robins and Delisi (1990). Thus, there are indications that ambient shear, under some conditions, can prolong vortex lifetime.

Final Comments

In summary, we believe that increasing ambient stratification or turbulence should decrease the maximum vortex migration distance and lifetime. On the other hand, increasing Reynolds number should increase H_{max} and T_{max}. Finally, increasing ambient shear should increase T_{max} but not necessarily H_{max}. It is clear that vortex evolution in realistic flows is a complex problem, and that our understanding is far from complete.

From a practical standpoint, the current state of our understanding of vortex wake behavior is important for assessing potential changes in commercial aircraft operations in the crowded airspace of busy airports. The results presented here have the following implications for both airport capacity and aircraft safety:

(a) It may be that, for practical purposes, a nonstratified, nonturbulent, nonsheared atmosphere rarely occurs. If it does occur, however, we should expect aircraft wake vortices to migrate significantly farther and last much longer than previous laboratory measurements would suggest.

(b) The classical view of the vortex hazard is one in which an aircraft encounters a vortex which is essentially straight and aligned with the aircraft flight path. The laboratory results suggest that for T greater than about 5 (corresponding to about 50 - 100 seconds for typical commercial aircraft) the encounter will be with a sinuous vortex or vortex ring which may significantly change the dynamics of the encounter. This effect is expected to occur sooner as ambient turbulence levels increase. It is not known to what degree, if any, this might be a function of Reynolds number.

(c) Although we cannot quantitatively describe the effects at this time, we should expect large variations in both vortex migration distance and lifetime with ambient background conditions.

(d) As implied above, the variations in vortex migration distance and lifetime may not correlate well with any single parameter.

(e) If accurate predictability of aircraft wake vortices is to be achieved, it will require a greater understanding of vortex evolution than currently available. From a practical standpoint, this implies that field studies will need to measure several atmospheric parameters simultaneously.

(f) The large scatter shown in Figures 9 and 10 indicate that, even under our controlled laboratory conditions, there is a random nature to vortex evolution. This scatter arises primarily from differences in the formation and evolution of

the three-dimensional vortices. Adding ambient stratification, turbulence, and shear will likely increase this late-wake scatter. Thus, we may ultimately have to accept a large uncertainty in our predictions of either migration distance or lifetime of aircraft wake vortices.

Acknowledgements

This study was supported by the Office of Naval Research under contracts N00014-89-C-0030 and N00014-88-C-0284 and by the Naval Sea Systems Command under contract N00024-91-C-6312.

REFERENCES

Aref, H. and Zawadzki, I., "Linking of Vortex Rings," *Nature*, Vol. 354, 1991, pp. 50-53.

Barker, S.J. and Crow, S.C., "The Motion of Two-Dimensional Vortex Pairs in a Ground Effect," *Journal of Fluid Mechanics*, Vol. 82, 1977, pp. 659-671.

Burnham, D.C., "B-747 Vortex Alleviation Flight Tests: Ground-Based Sensor Measurements," U.S. Dept. of Transportation, Federal Aviation Administration, Rept. DOT-FAA-RD-81-99, 1982.

Burnham, D.C., Hallock, J.N., Tombach, I.H., Brashears, M.R., and Barber, M.R. "Ground-Based Measurements of the Wake Vortex Characteristics of a B-747 Aircraft in Various Configurations," U.S. Dept. of Transportation, Federal Aviation Admin. Report DOT-TSC-FAA-78-28, 1978.

Condit, P.M., and Tracy, P.W., "Results of the Boeing Company Wake Turbulence Test Program," *Aircraft Wake Turbulence and Its Detection*, edited by J.H. Olsen, A. Goldburg, and M. Rogers, Plenum, New York, 1971, pp. 473-508.

Crow, S.C., "Stability Theory for a Pair of Trailing Vortices," *AIAA Journal*, Vol. 8, 1970, pp. 2172-2179.

Delisi, D.P., and Dunkerton, T.J., "Laboratory Observations of Gravity Wave Critical-Layer Flows," *Pure and Applied Geophysics*, Vol. 130, 1989, pp. 445-461.

Delisi, D.P., and Greene, G.C., "Measurements and Implications of Vortex Motions Using Two Flow-Visualization Techniques," *Journal of Aircraft*, Vol. 27, 1990, pp. 968-971.

Delisi, D.P., and Orlanski, I., "On the Role of Density Jumps in the Reflection and Breaking of Internal Gravity Waves," *Journal of Fluid Mechanics*, Vol. 69, 1975, pp. 445-464.

Delisi, D.P., Robins, R.E., and Lucas, R.D., "Initial Laboratory Observations of the Evolution of a Vortex Pair In a Stratified Shear Flow," *Physics of Fluids* A, 1991, in press.

Glezer, A. and D. Coles, "An Experimental Study of a Turbulent Vortex Ring," *J. Fluid Mech.*, 1990, pp. 243-283.

Greene, G.C., "An Approximate Model of Vortex Decay in the Atmosphere," *Journal of Aircraft*, Vol. 23, July 1986, pp. 566-573.

Hall, M.G., "Vortex Breakdown," *Annual Reviews of Fluid Mechanics*, Vol. 4, 1972, pp. 195-218.

Leibovich, S., "The Structure of Vortex Breakdown," *Annual Reviews of Fluid Mechanics*, Vol. 10, 1978, pp. 221-246.

Olsen, J.H., Goldburg, A., and Rogers, M., *Aircraft Wake Turbulence and Its Detection*, Plenum Press, New York, 1971.

Robins, R.E. and Delisi, D.P., "Numerical Study of Vertical Shear and Stratification Effects On the Evolution of a Vortex Pair," *AIAA Journal*, Vol. 28, 1990, pp. 661-669.

Saffman, P.G., and Baker, G.R., "Vortex Interactions," *Annual Reviews of Fluid Mechanics*, Vol. 11, 1979, pp. 95-122.

Sarpkaya, T., "Trailing Vortices in Homogeneous and Density-Stratified Media," *Journal of Fluid Mechanics*, Vol. 136, 1983, pp. 85-109.

Sarpkaya, T., "Computational Methods With Vortices - The 1988 Freeman Scholar Lecture," *Journal of Fluids Engineering*, Vol. 111, 1989, pp. 5-52.

Sarpkaya, T., and Daly, J.J., "Effect of Ambient Turbulence on Trailing Vortices," *Journal of Aircraft*, Vol. 24, 1987, pp. 399-404.

Schatzle, P.R., "An Experimental Study of Fusion of Vortex Rings," Ph.D. Thesis, California Inst. of Tech., Pasadena, CA, 1987.

Scorer, R.S., *Natural Aerodynamics*, Pergamon Press, New York, 1958.

Smith, J.H.B., "Vortex Flows in Aerodynamics," *Annual Reviews of Fluid Mechanics*, Vol. 18, 1986, pp. 221-242.

Tomassian, J.D., "The Motion of a Vortex, Pair in a Stratified Medium," Ph.D. Thesis, Univ. of California, Los Angeles, CA, 1979.

Tombach, I.H., "Observations of Atmospheric Effects on Vortex Wake Behavior," *Journal of Aircraft*, Vol. 10, 1973, pp. 641-647.

Widnall, S.E., "The Structure and Dynamics of Vortex Filaments," *Annual Reviews of Fluid Mechanics*, Vol. 7, 1975, pp. 141-165.

LIST OF TABLES

1. The physical parameters of the wings used in this study and the maximum chord Reynolds numbers.

FIGURE CAPTIONS

1. Streak photograph of a trailing wake vortex using uniformly seeded particles.

2. Lift, normalized by the lift at a depth of two spans, vs trailing edge depth. Data shown are for the 10.2 cm span wing at towing speeds of 324 cm/sec (diamonds) and 201 cm/sec (triangles) and for the 5.1 cm span wing at towing speeds of 324 cm/sec (squares) and 201 cm/sec (circles).

3. Dye measurements for nonstratified flow from Tomassian (1979; plus symbols), Sarpkaya (1983; Xs), and Delisi and Greene (1990; circles).

4. Streak photographs for the 5.1 cm span wing at an angle of 13 deg and a towing speed of 324 cm/sec. Values of T are: (a) 2.8, (b) 5.3, (c) 7.8, (d) 10.3, (e) 12.8, (f) 15.3, (g) 17.8, and (h) 20.2.

5. Drawings of the flow field shown in Figure 4 at two times in the evolution of a vortex wake. Figures 5a and 5b show the three-dimensional and side view, respectively, of the flow field at an early time, while the wake is two dimensional. Figures 5c and 5d show the corresponding views at a later time, after the wake has evolved into three-dimensional ring vortices.

6. Photographs of the bottom floor with an initially uniform distribution of particles. Data are for the 10.2 cm span wing at a towing speed of 200 cm/sec. The distance of the wing above the floor was (a) 2.5 spans, (b) 5 spans, and (c) 8 spans.

7. H vs T for the run shown in Fig 4. The letters correspond to the photographs in Fig. 4. For this experiment, the bottom floor is at H ≈ .

8. H vs T for a typical run. For this experiment, the bottom floor is at H ≈ .

9. H vs T for the 5.1 cm span wing using particle streak measurements at towing speeds of 324 cm/sec (circles), 232 cm/sec (squares), and 176 cm/sec (triangles). The bottom floor is at H ≈ .

10. H vs T for the 3.8 cm span wing using particle streak measurements at a towing speed of 324 cm/sec. The bottom floor is at H ≈ 22 or H ≈ 17.

11. Traces of the bottom of the region containing particles for the photographs in Figure 4.

12. Bottom particle traces showing merging of the vortex rings.

13. Distance between rings normalized by b_0, d / b_0, for the experiment of Fig. 12.

14. Distance between rings d / b_0, for all 3.8 cm span wing runs.

15. Distance between rings, d / b_0, for all 5.1 cm span wing runs.

16. Distance between rings, d / b_0, vs wing span at $T \approx 11$. Error bars indicate $\pm$ one standard deviation.

17. Diameters of ring vortices, normalized by b_0, D / b_0, vs T for the 3.8 cm span wing (circles) and the 5.1 cm span wing (squares). Solid symbols are rings that have merged and re-formed.

18. Nondimensional times, T, of the first visual observation of an instability in the two-dimensional flow and the times when the three-dimensional ring vortices appear fully formed. The observations were from the side of the tank using particles for flow visualization. Circles (squares) are for experiments with the 3.8 (5.1) cm span wing.

TABLE 1

Wing Type	Span (cm)	Chord (cm)	Plate Thickness (cm)	Max. Airfoil Thickness From Baseline (cm)	Max. Reynolds Number Re_c
Circular Arc	9.90	5.84		0.64	189,200
Circular Arc	7.62	4.57		0.66	91,400
Curved Plate	5.08	2.54	0.056	0.28	82,300
Curved Plate	3.81	1.90	0.056	0.22	61,600

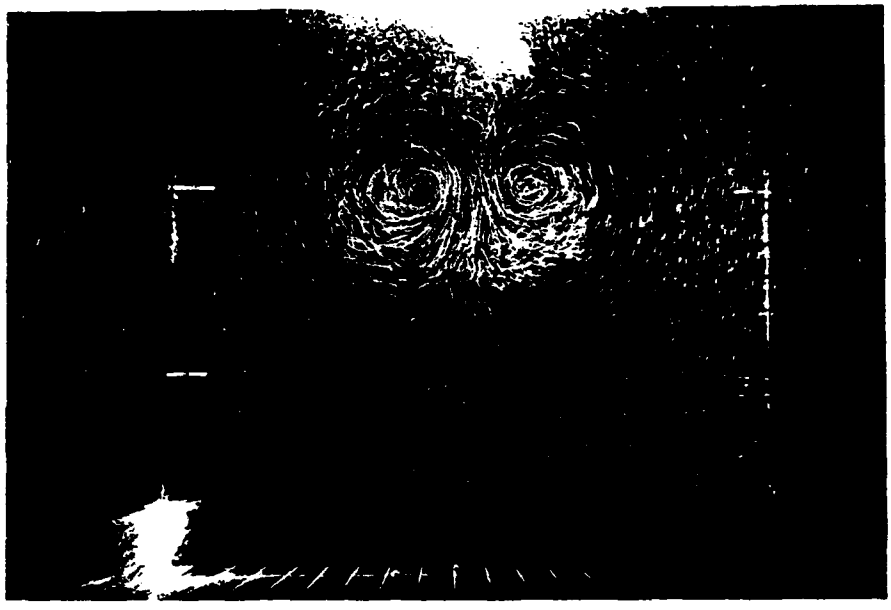

Figure 1

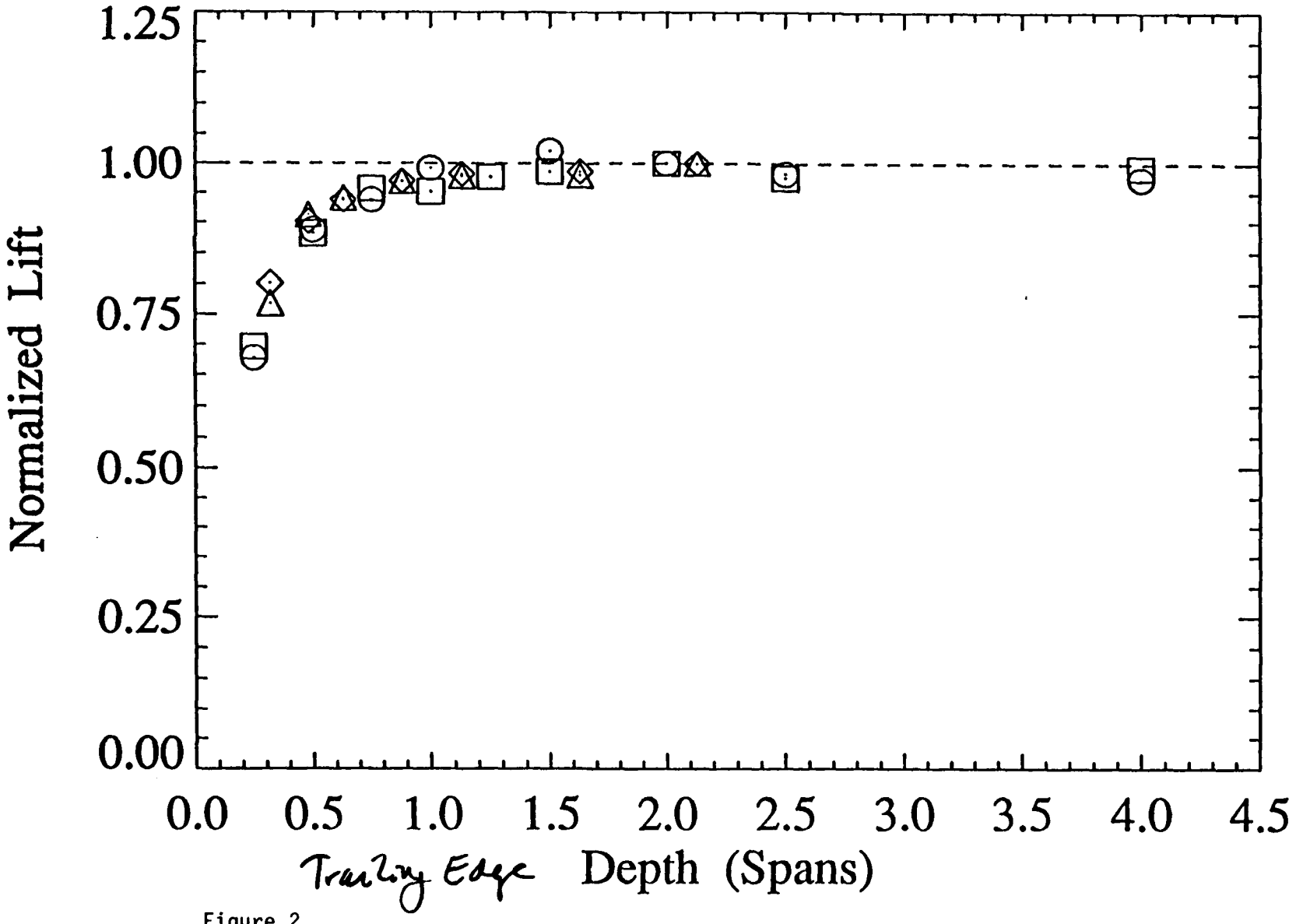
Normalized Lift
1.25
1.00
0.75
0.50
0.25
0.00
0.0
0.5
1.0
1.5
2.0
2.5
3.0
3.5
4.0
4.5
Trailing Edge Depth (Spans)

Figure 2

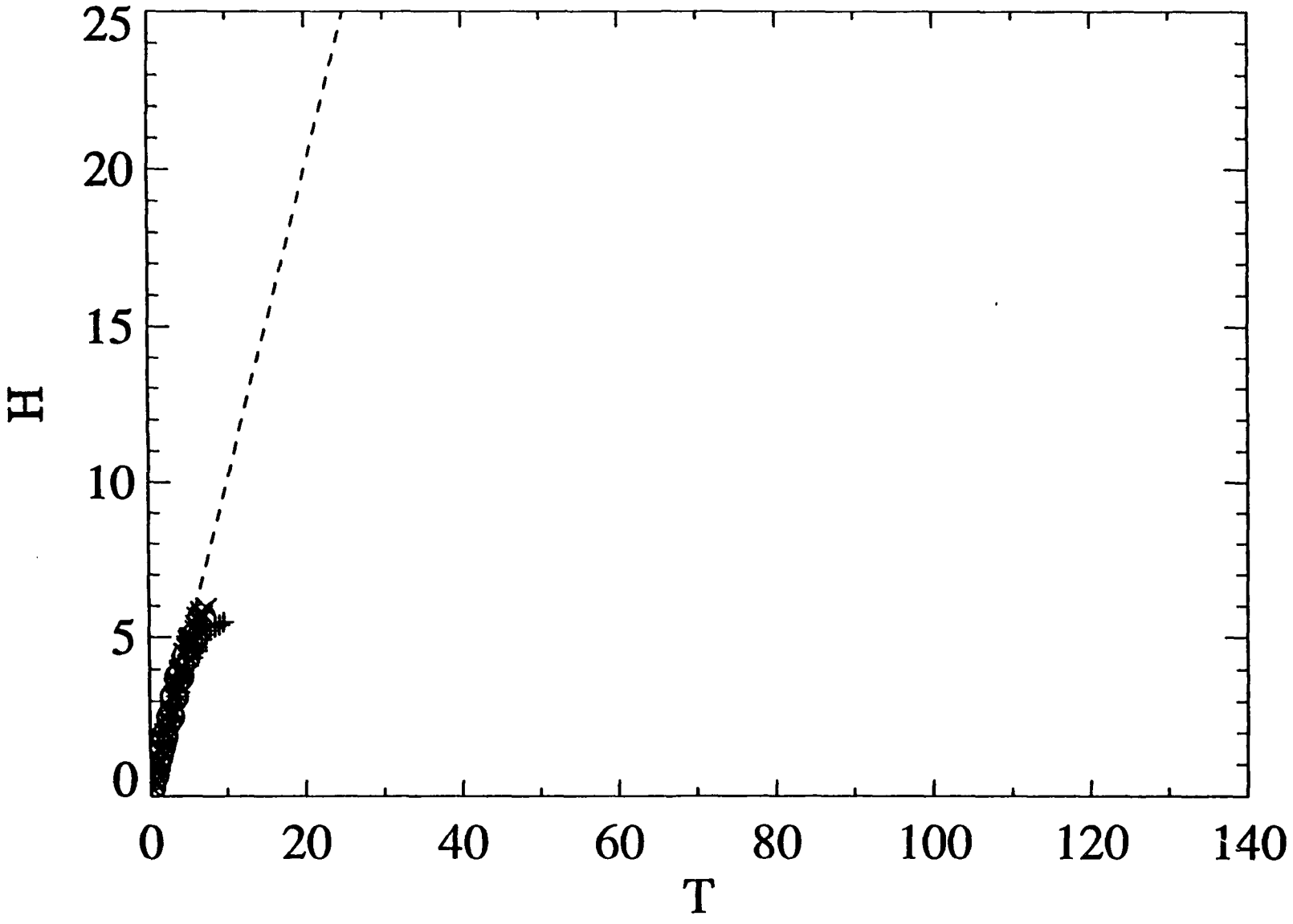

Figure 3

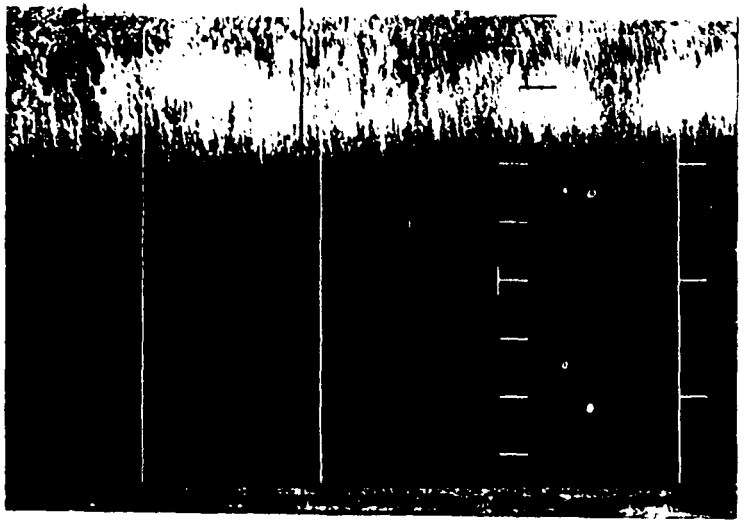

Figure 4a

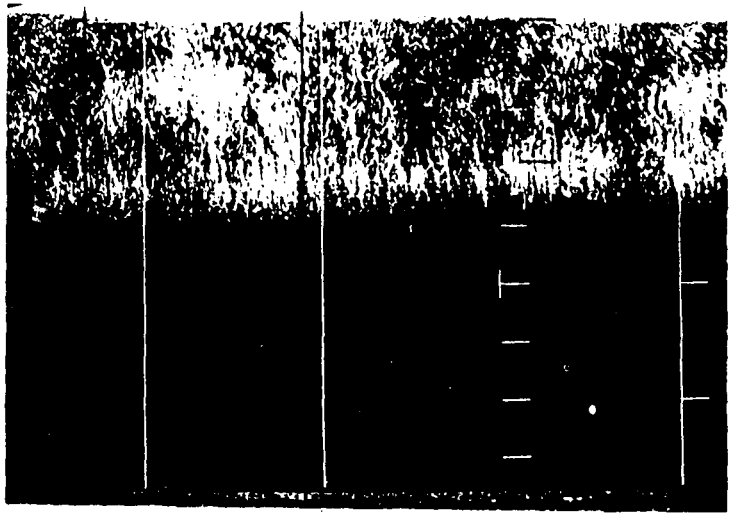

Figure 4b

Figure 4c

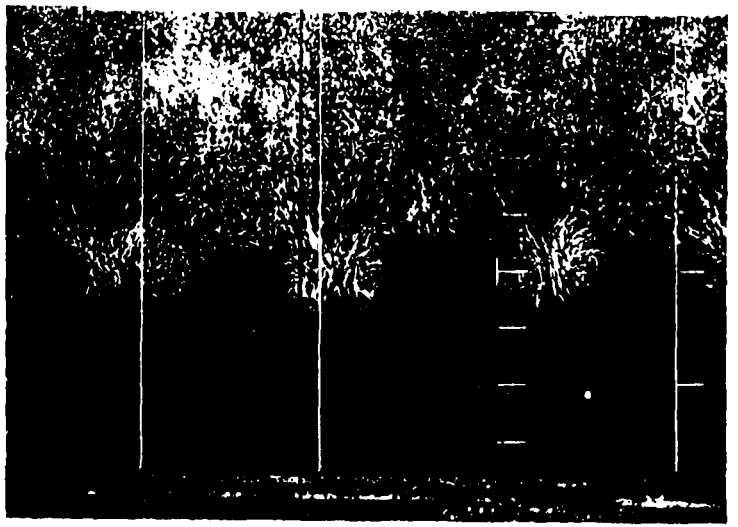

Figure 4d

Figure 4e

Figure 4f

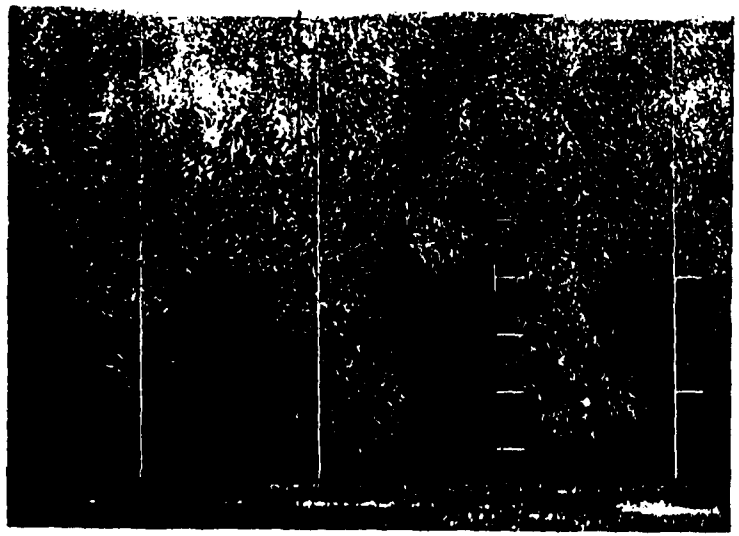

Figure 4g

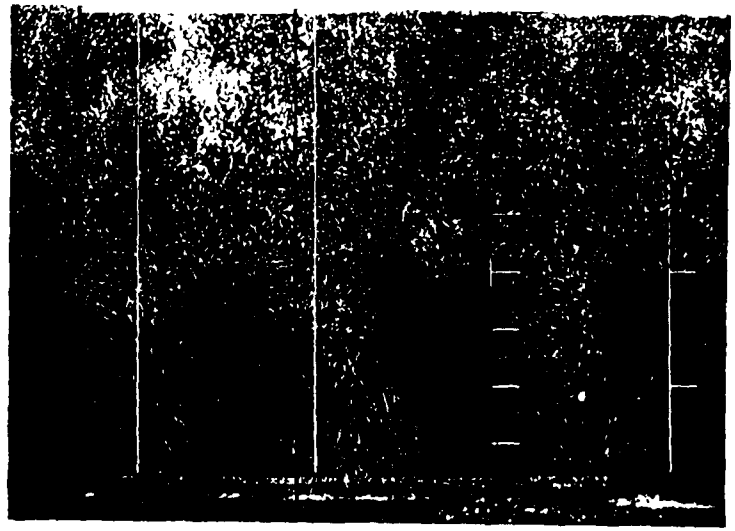

Figure 4h

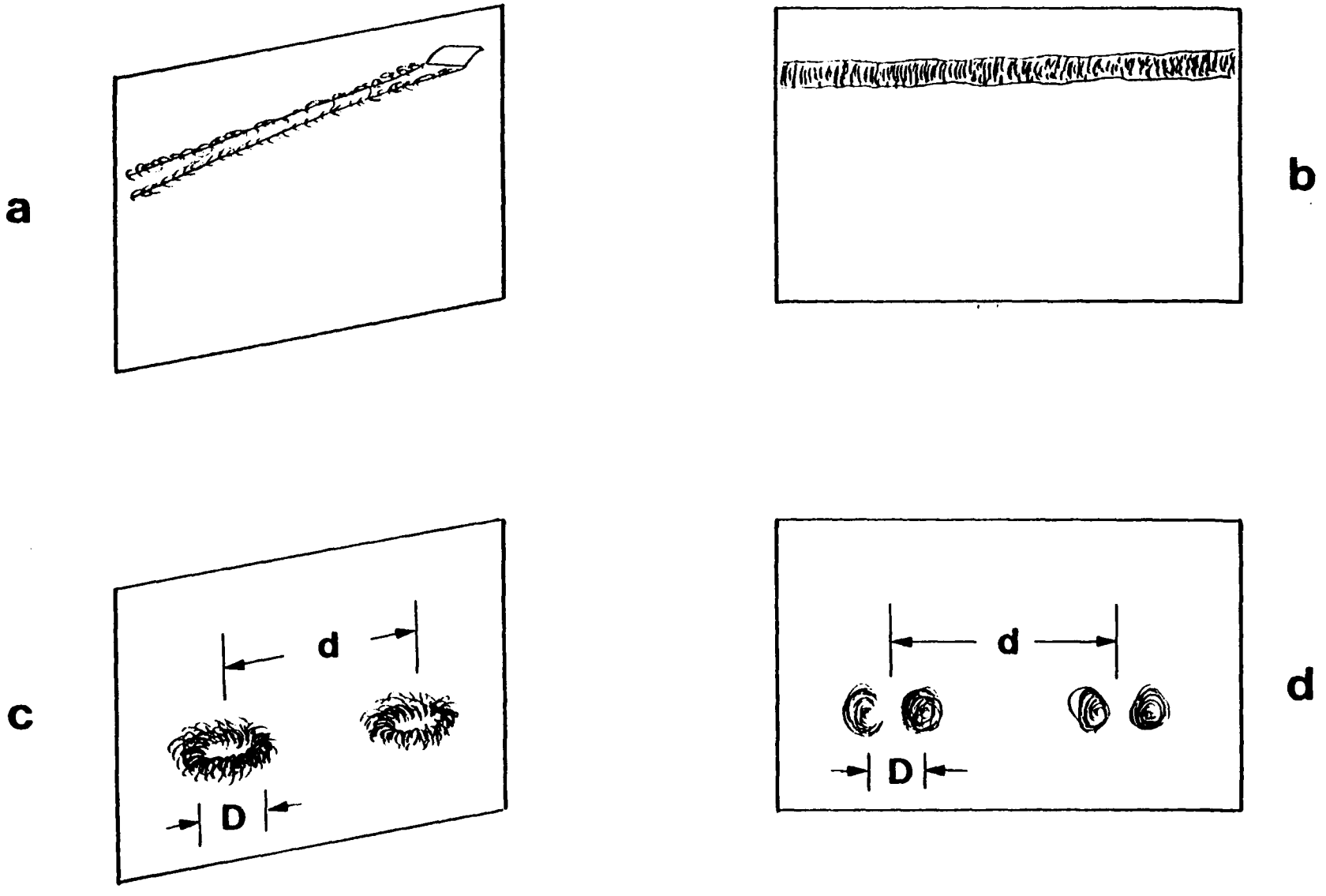

Figure 5

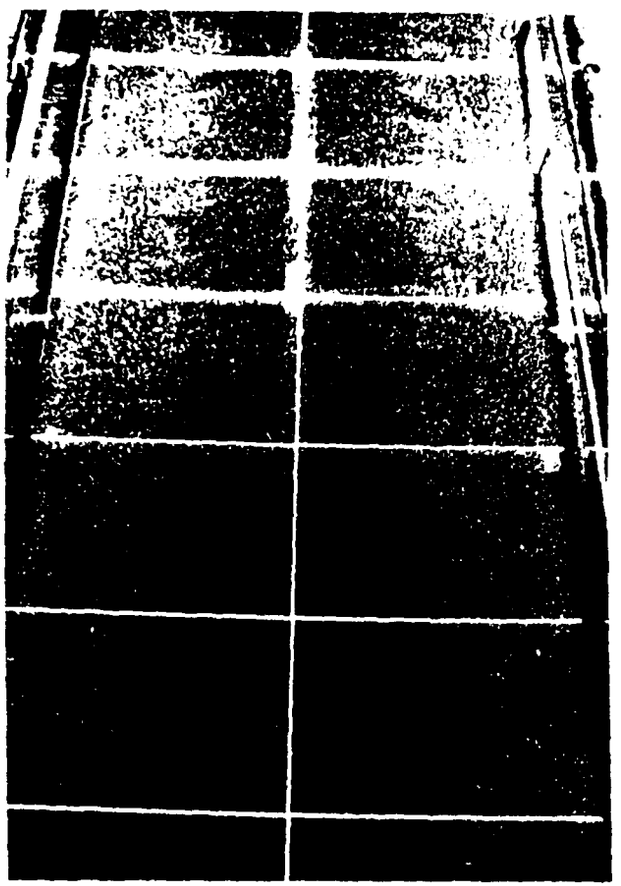

Figure 6a

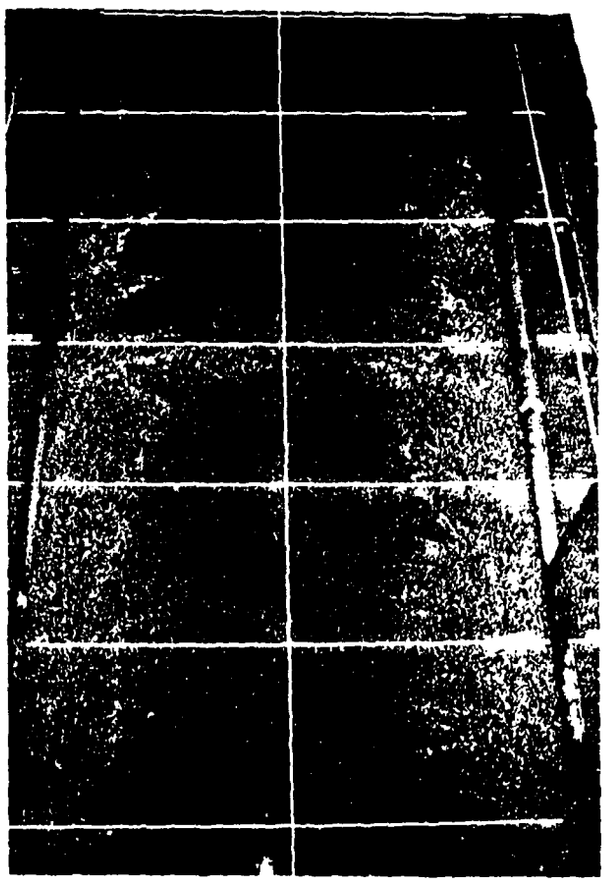

Figure 6b

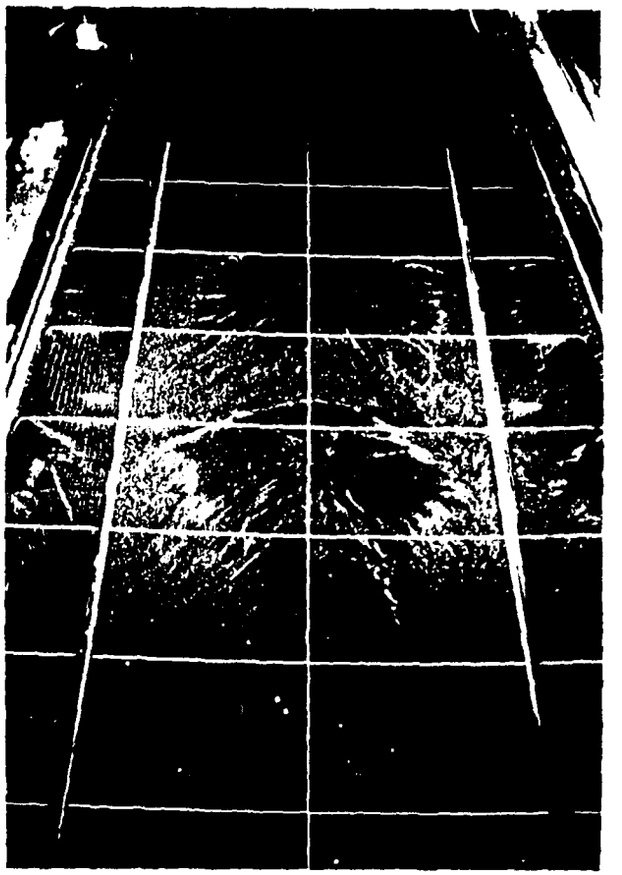

Figure 6c

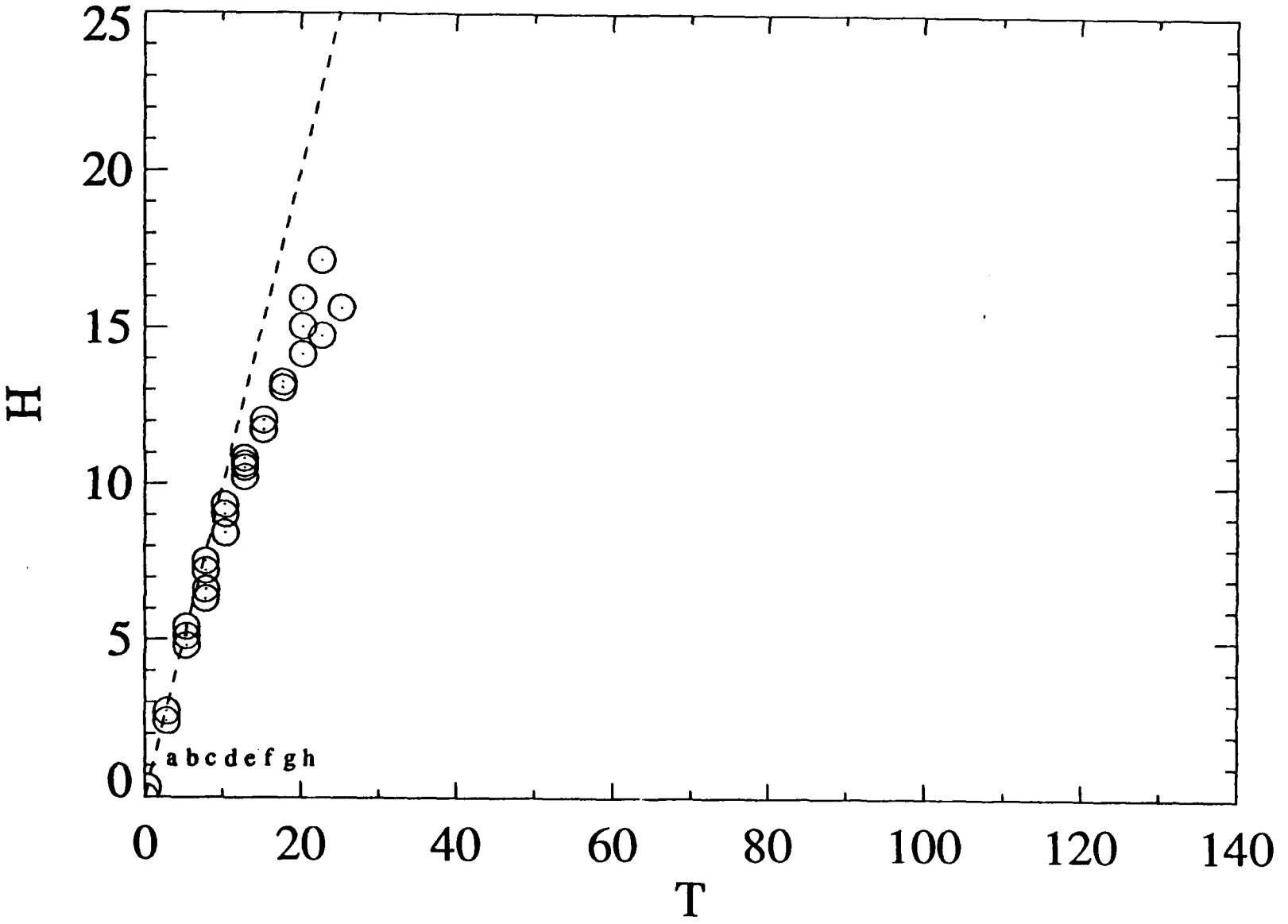

Figure 7

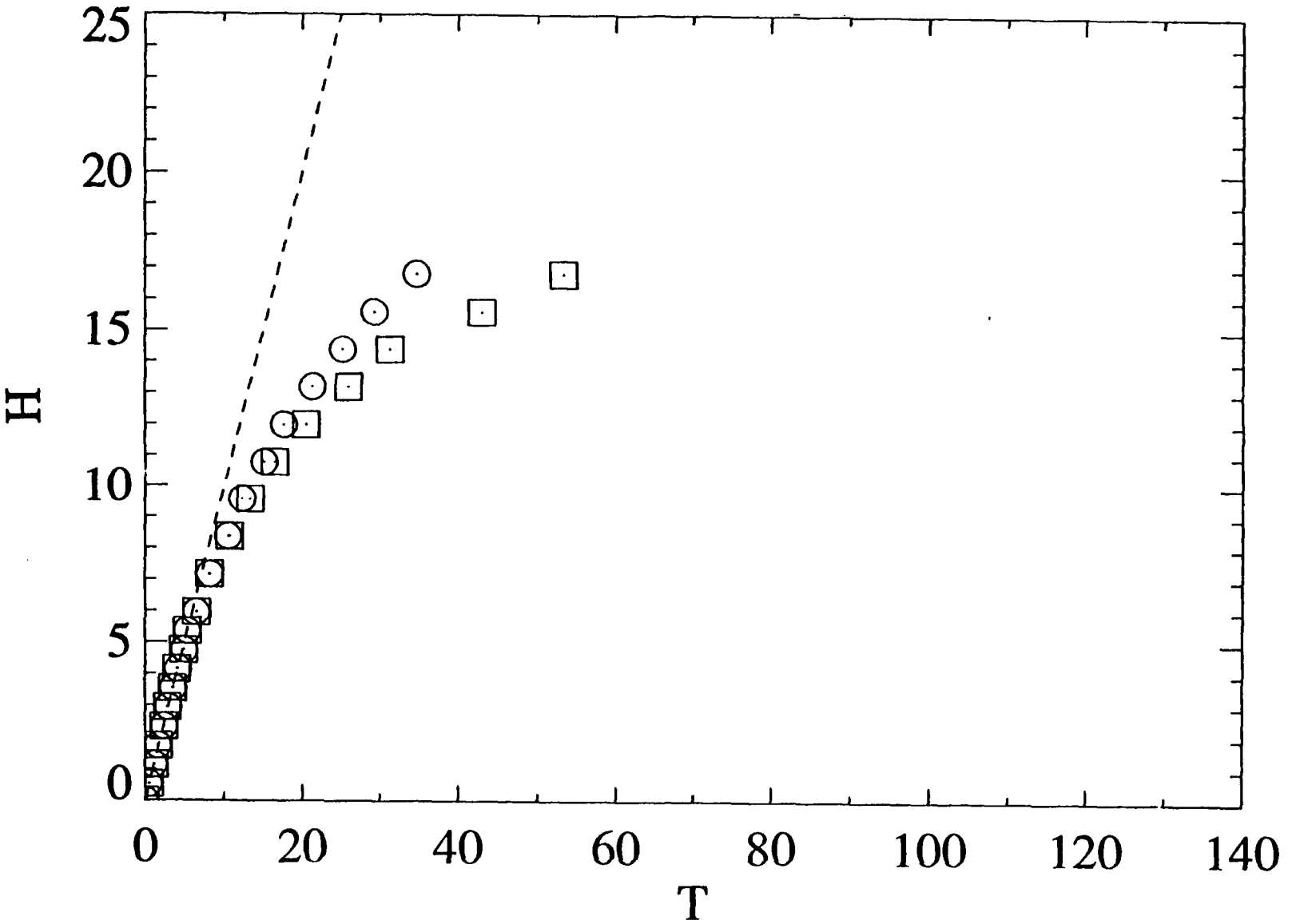

Figure 8

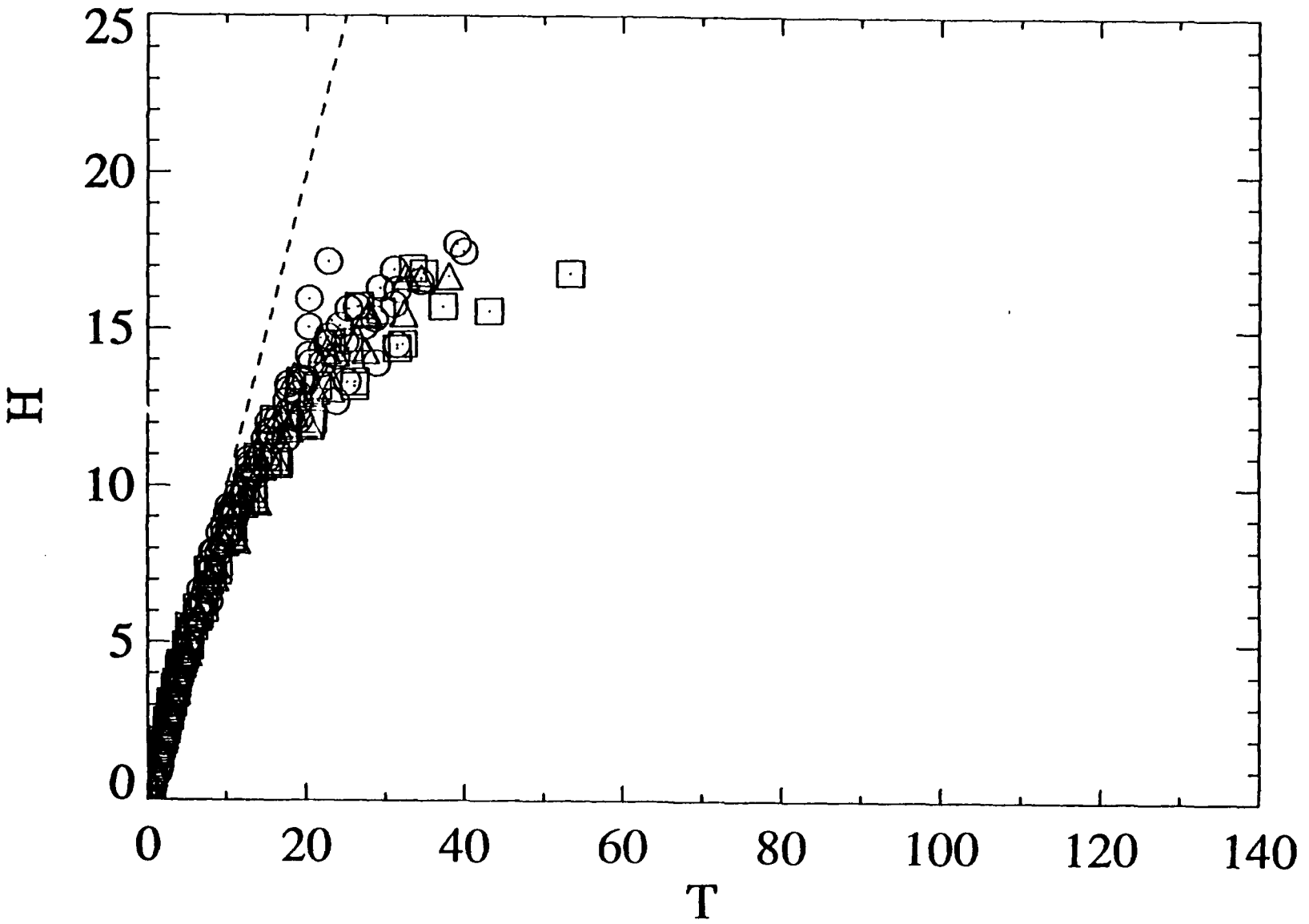

Figure 9

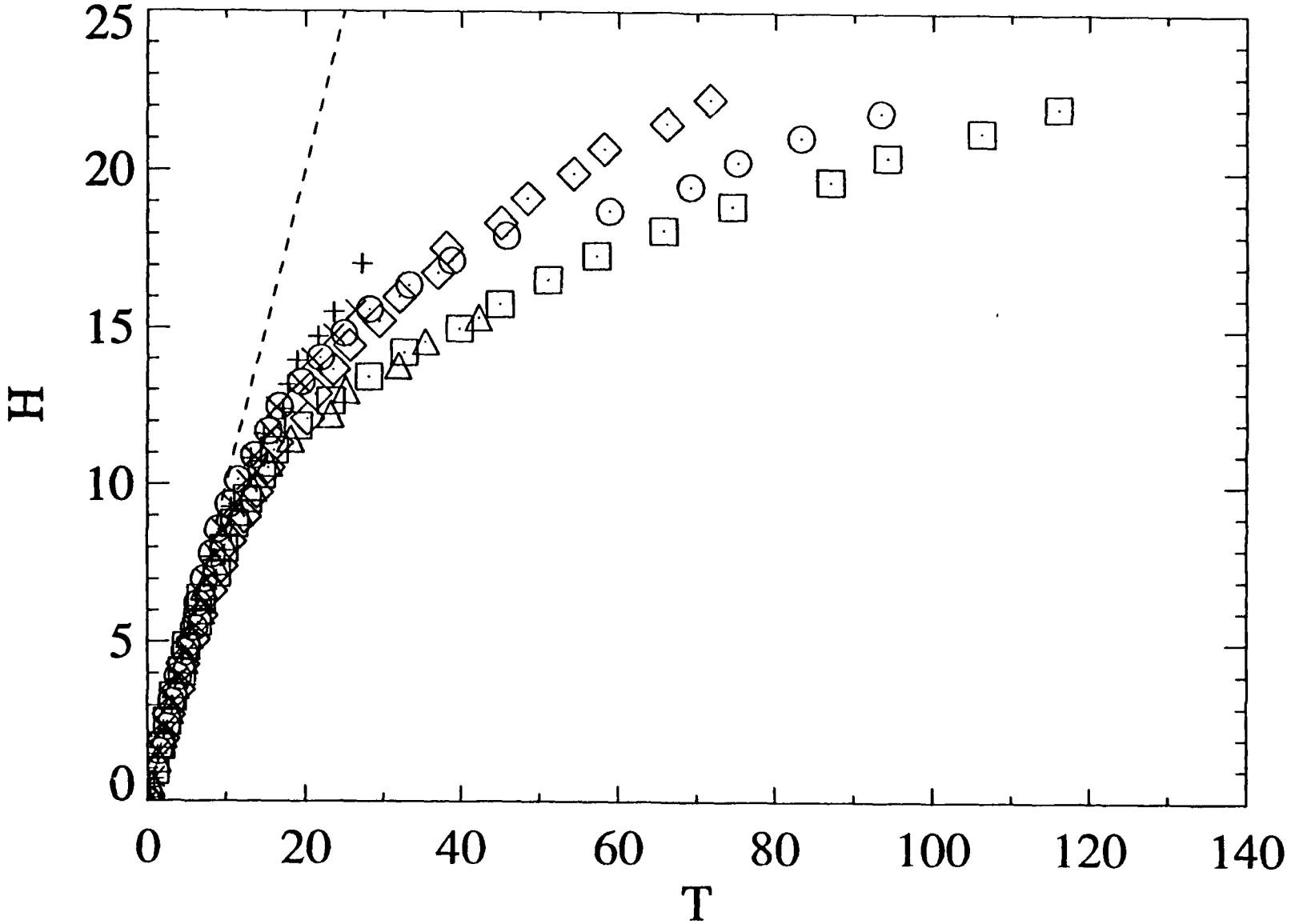

Figure 10

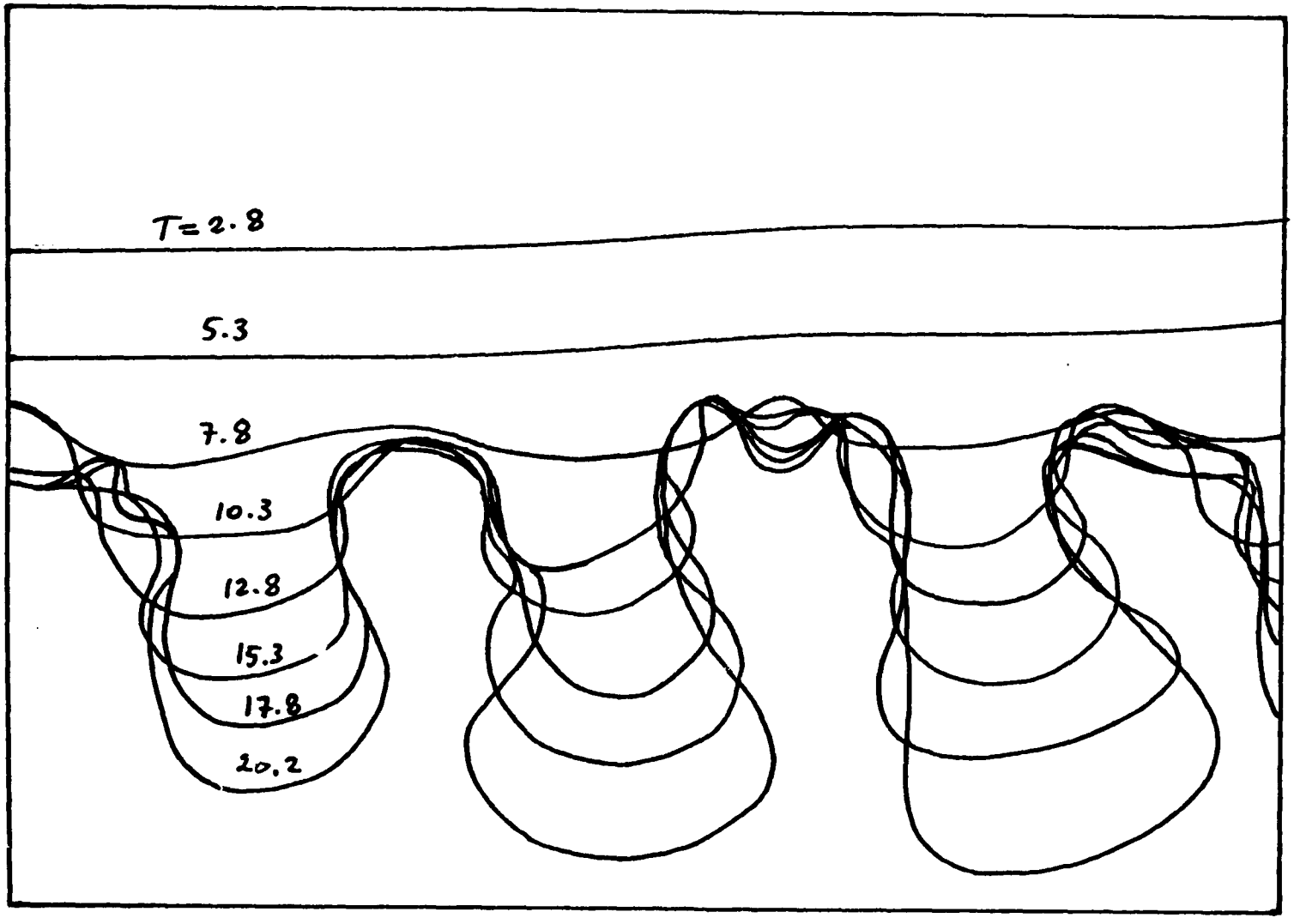

Figure 11

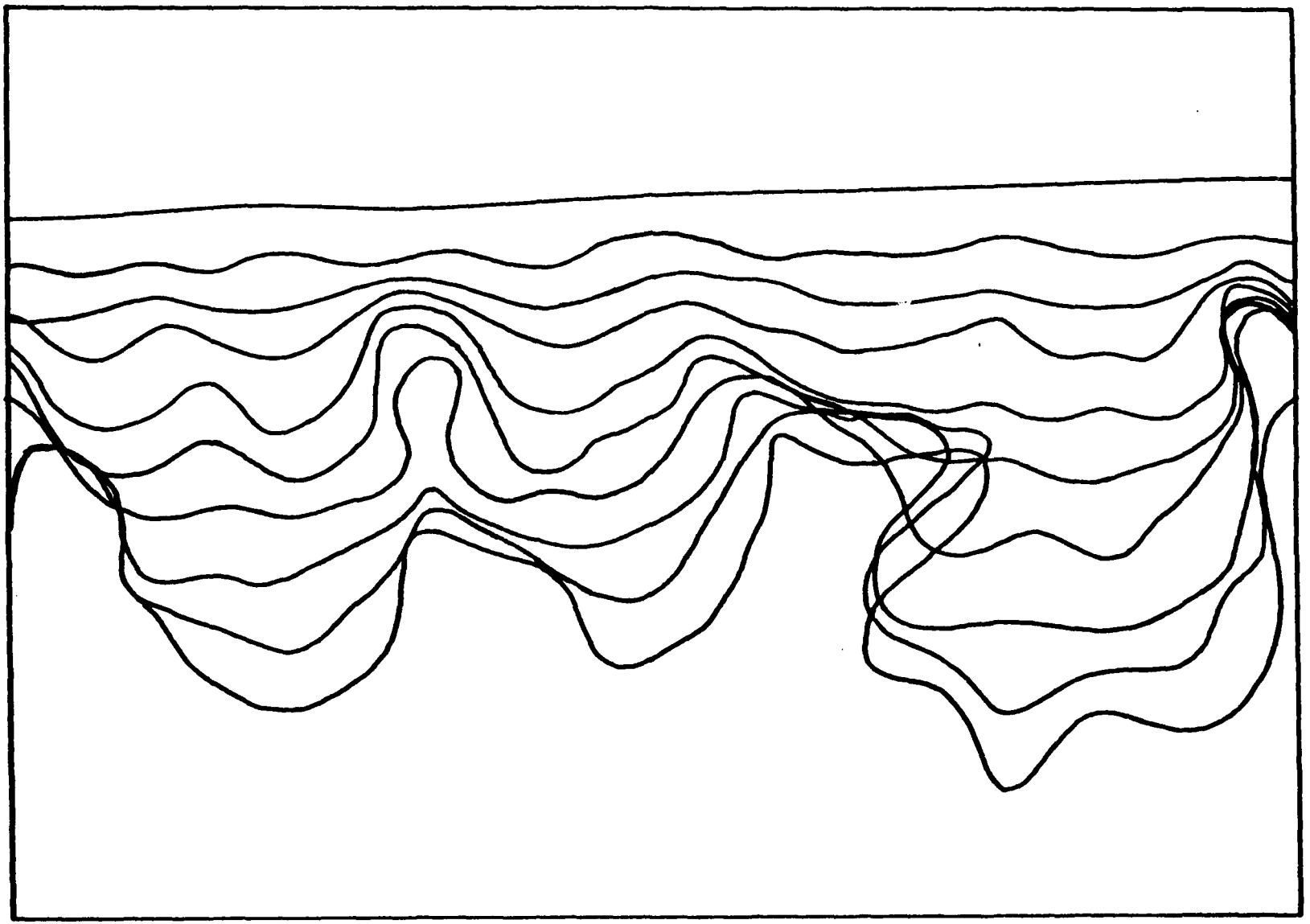

Figure 12

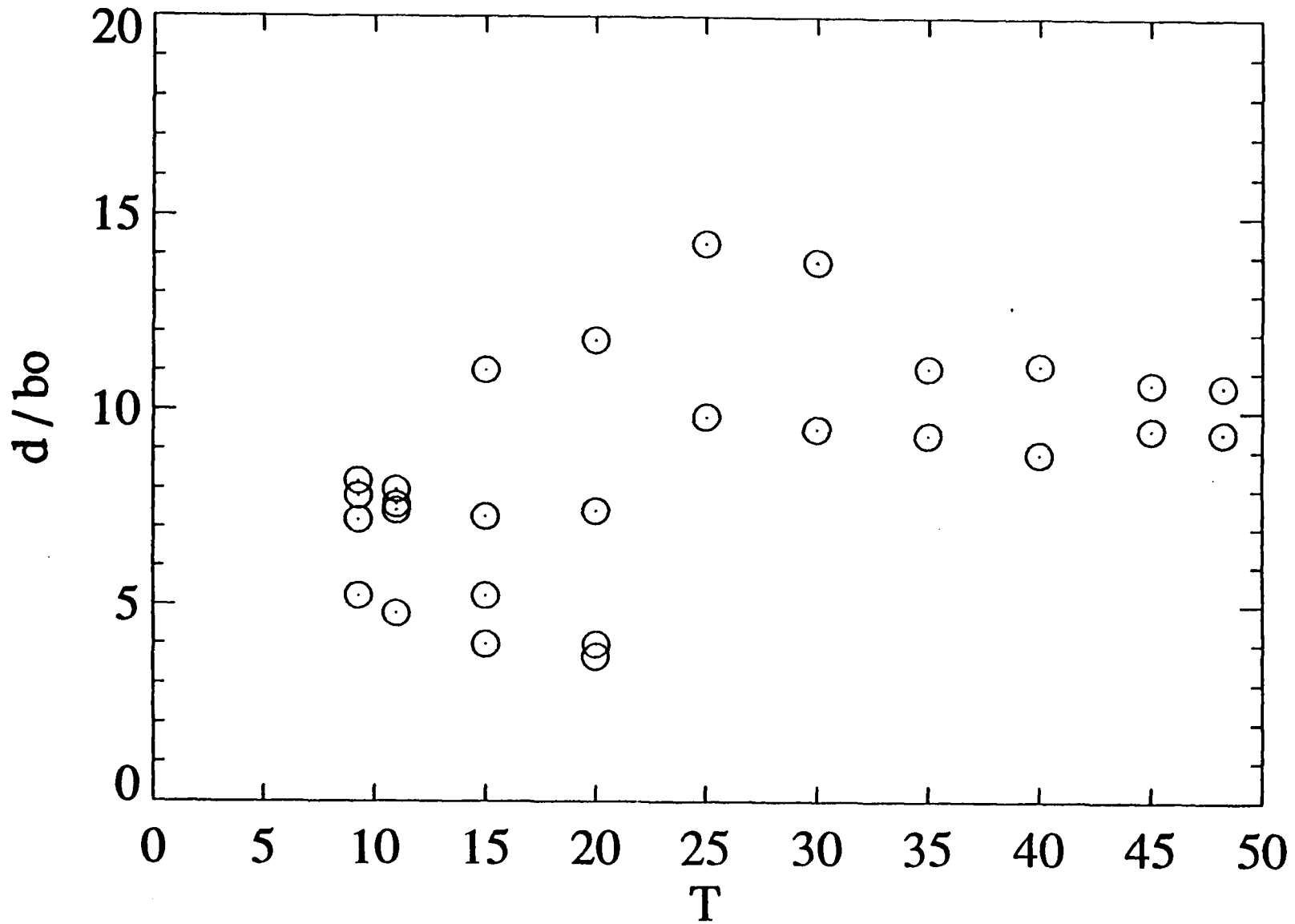

Figure 13

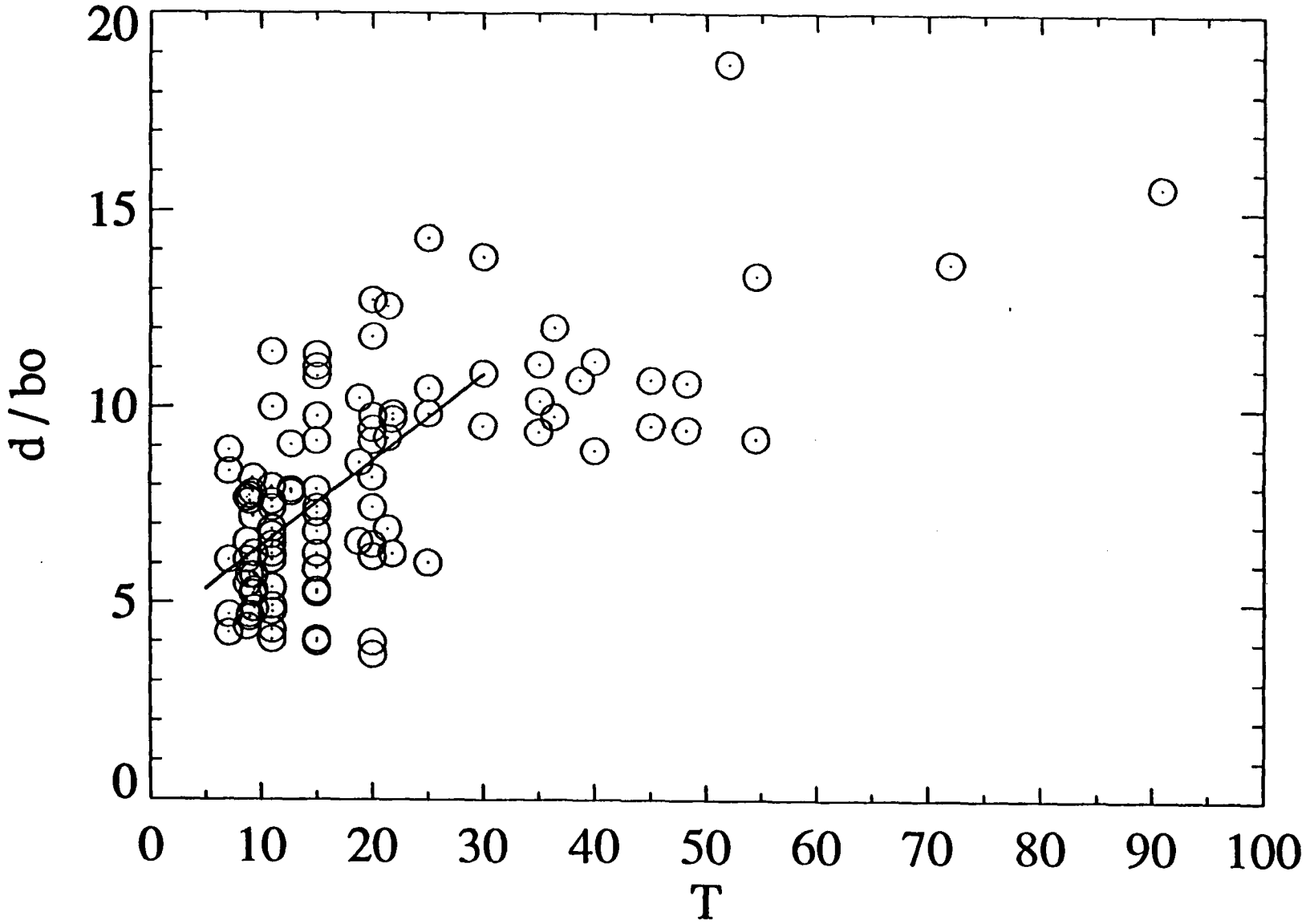

Figure 14

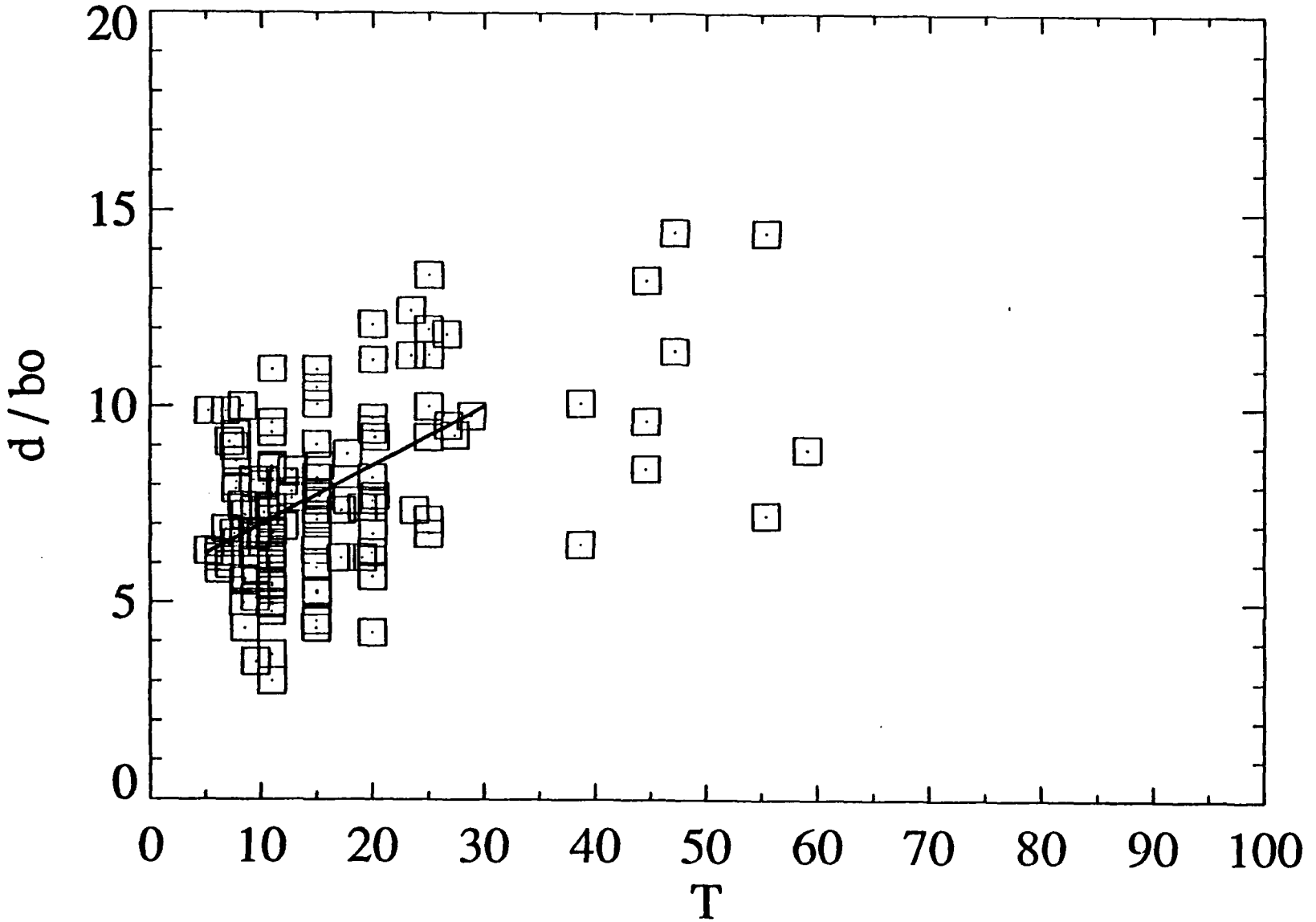

Figure 15

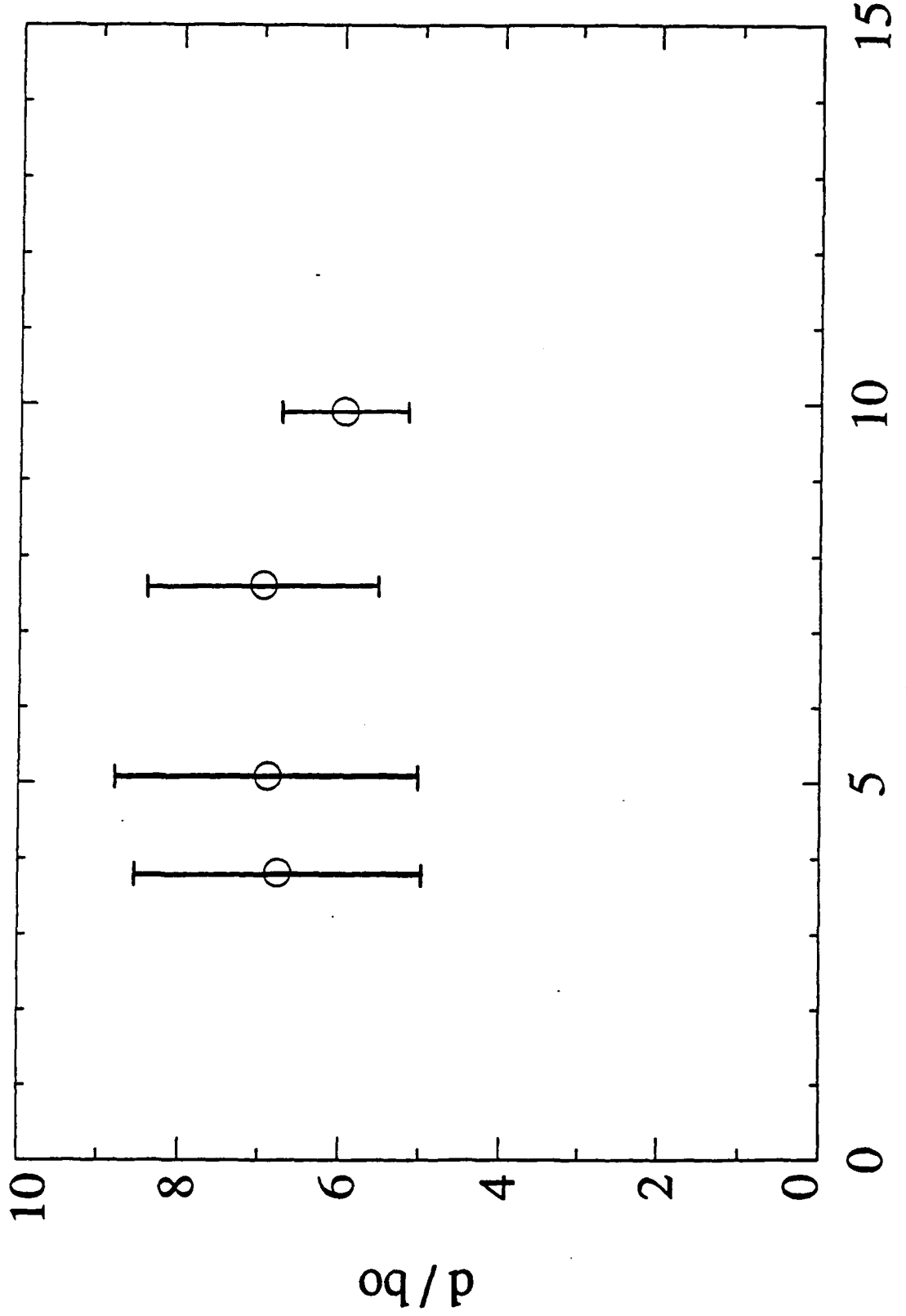

Figure 16

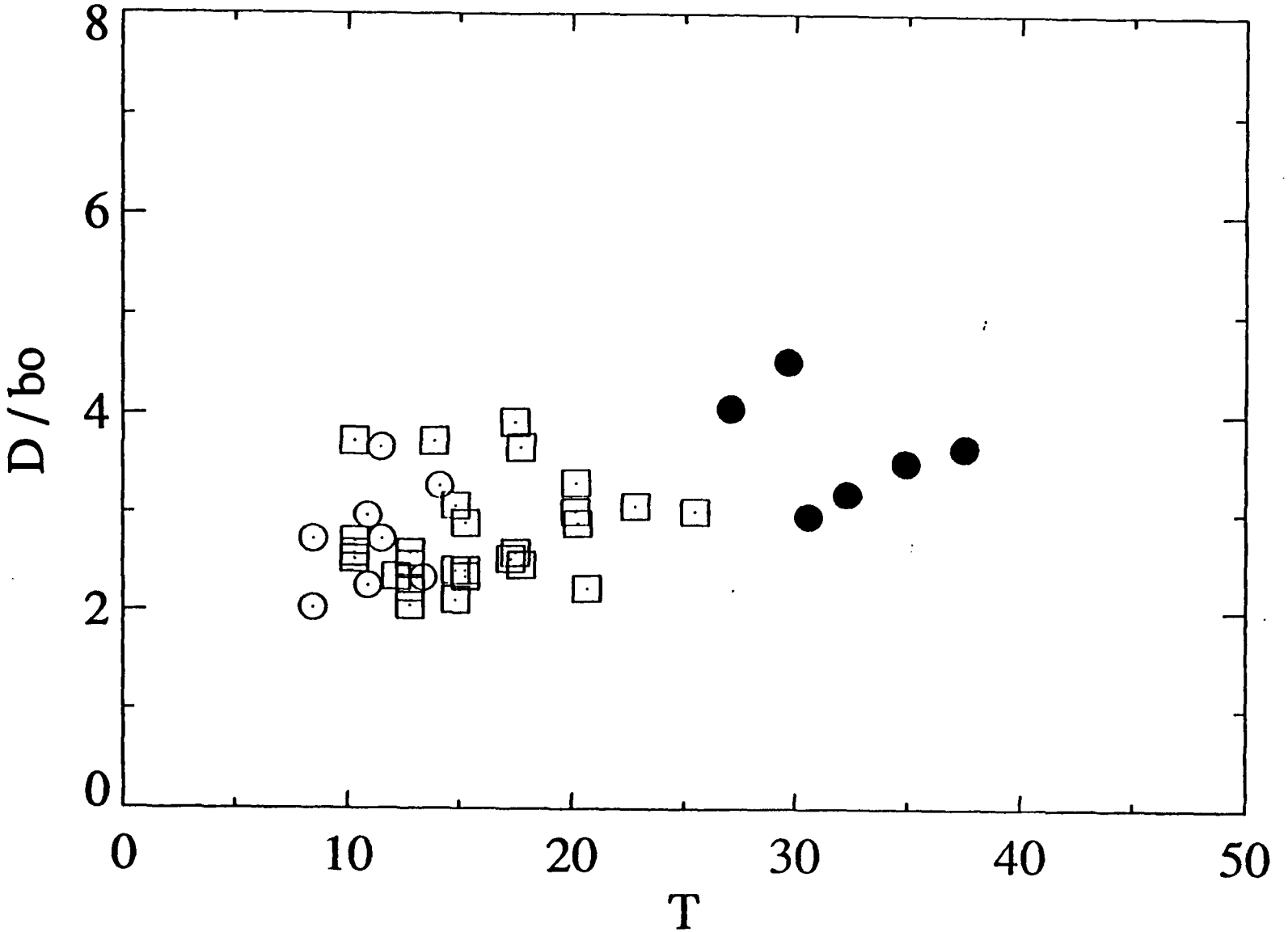

Figure 17

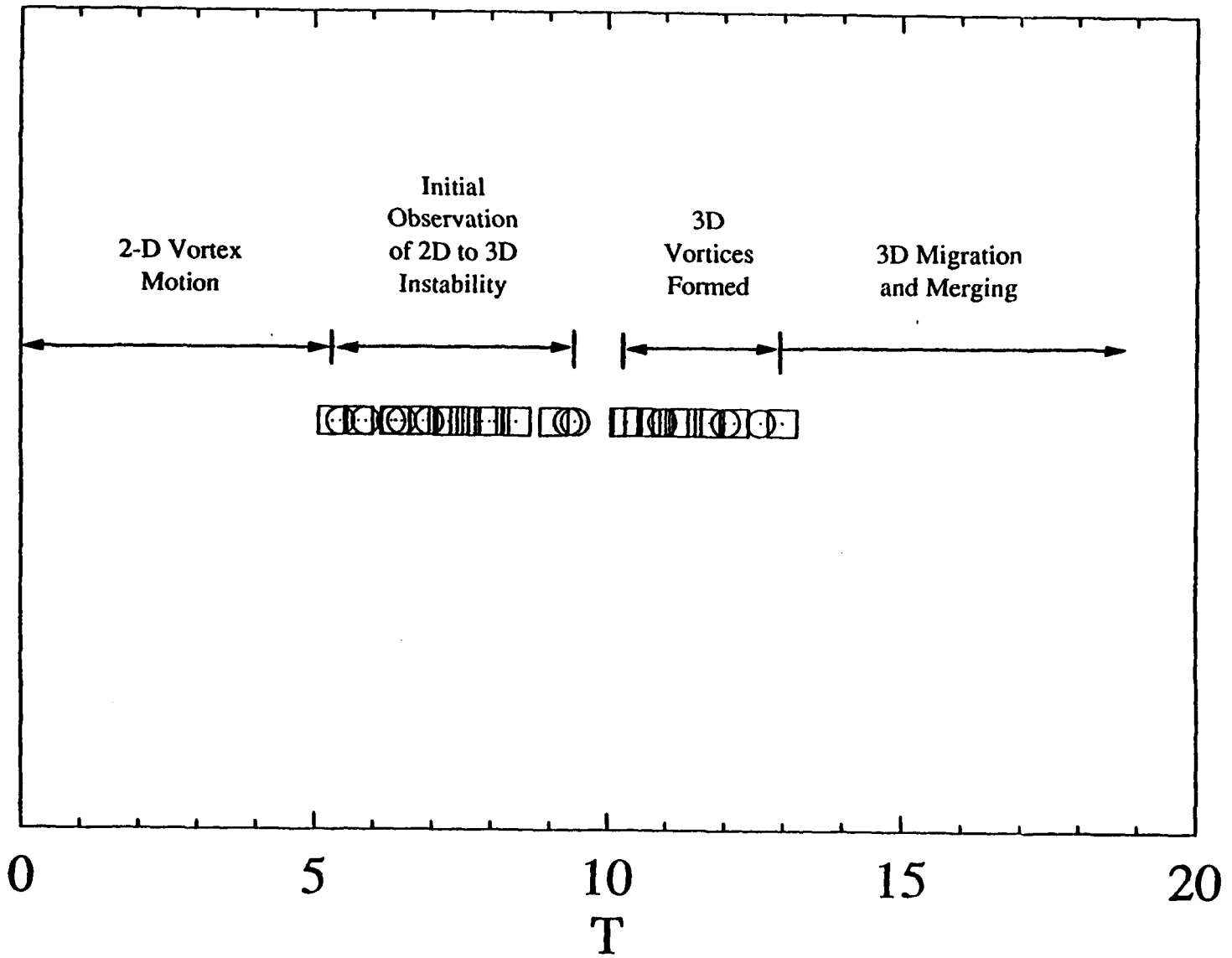
2-D Vortex Motion
Initial Observation of 2D to 3D Instability
3D Vortices Formed
3D Migration and Merging
0
5
10
15
20
T

Figure 18